A Climatology of Marine Boundary Layer Cloud and Drizzle Properties Derived from Ground-Based Observations over the Azores

PENG WU,[a] XIQUAN DONG, AND BAIKE XI

Department of Hydrology and Atmospheric Sciences, The University of Arizona, Tucson, Arizona

(Manuscript received 16 April 2020, in final form 28 July 2020)

ABSTRACT: In this study, more than 4 years of ground-based observations and retrievals were collected and analyzed to investigate the seasonal and diurnal variations of single-layered MBL (with three subsets: nondrizzling, virga, and rain) cloud and drizzle properties, as well as their vertical and horizontal variations. The annual mean drizzle frequency was ~55%, with ~70% in winter and ~45% in summer. The cloud-top (cloud-base) height for rain clouds was the highest (lowest), resulting in the deepest cloud layer, i.e., 0.8 km, which is 4 (2) times that of nondrizzling (virga) clouds. The retrieved cloud-droplet effective radii r_c were the largest (smallest) for rain (nondrizzling) clouds, and the nighttime values were greater than the daytime values. Drizzle number concentration N_d and liquid water content LWC$_d$ were three orders and one order lower, respectively, than their cloud counterparts. The r_c and LWC$_c$ increased from the cloud base to $z_i \approx 0.75$ by condensational growth, while drizzle median radii r_d increased from the cloud top downward the cloud base by collision–coalescence. The adiabaticity values monotonically increased from the cloud top to the cloud base with maxima of ~0.7 (0.3) for nondrizzling (rain) clouds. The drizzling process decreases the adiabaticity by 0.25 to 0.4, and the cloud-top entrainment mixing impacts as deep as upper 40% of the cloud layers. Cloud and drizzle homogeneities decreased with increased horizontal sampling lengths. Cloud homogeneity increases with increasing cloud fraction. These results can serve as baselines for studying MBL cloud-to-rain conversion and growth processes over the Azores.

KEYWORDS: Clouds; Drizzle; Marine boundary layer; Cloud retrieval; Databases; Surface observations

1. Introduction

Owing to their high albedo and close vicinity to the surface, marine boundary layer (MBL) clouds strongly reflect shortwave radiation while having little effect on the outgoing longwave radiation, thus imposing a strong cooling effect onto the underlying surface (Randall et al. 1984; Slingo 1990). MBL clouds cover vast areas of the eastern subtropical oceans and over midlatitude oceans, making them a key component in Earth's radiation budget (Klein et al. 1993; Bony and Dufresne 2005; Wood et al. 2009). Despite their importance, climate models often underestimate low cloud cover but overestimate their optical thickness (Nam et al. 2012; Bony and Dufresne 2005) and simulate different signs and magnitudes of the low cloud feedback (Zelinka et al. 2020; Vial et al. 2013; Bony and Dufresne 2005).

MBL clouds frequently produce precipitation, most often in the form of drizzle (Wood 2012; Rémillard et al. 2012; Dong et al. 2014a; Wu et al. 2015, 2017), and drizzle can strongly modulate stratocumulus-to-cumulus transition (Yamaguchi et al. 2017). The presence of drizzle adds extra complexity in simulating MBL clouds. For example, climate models simulate overly frequent but light precipitation in low clouds compared with observations (Lebsock et al. 2013; Dolinar et al. 2015). This is partially attributed to lack of reliable subgrid variations of MBL cloud and precipitation microphysics in climate models (Lebsock et al. 2013; Xie and Zhang 2015; Wu et al. 2018; Wang et al. 2019). Besides their spatial variations, the vertical distributions of MBL cloud and drizzle microphysical properties are also crucial in simulating precipitation rate.

The collision–coalescence process is usually partitioned into autoconversion and accretion subprocesses in numerical models and are often parameterized as power-law relationships of cloud droplet effective radius (r_c), number concentration (N_c), liquid water content (LWC$_c$; or cloud water mixing ratio, q_c) and of drizzle drop size (r_d), number concentration (N_d), and liquid water content (LWC$_d$; or drizzle water mixing ratio, q_d) (Liu and Daum 2004; Liu et al. 2006, 2007; Khairoutdinov and Kogan 2000; Beheng 1994; Tripoli et al. 1980). Not only are the variations in individual quantities important, but additionally the covariances between multiple microphysical properties are important in predicting reasonable precipitation frequency and intensity (Lebsock et al. 2013; Xie and Zhang 2015; Wu et al. 2018; Wang et al. 2019). Regions or periods with higher covariance of q_c and q_d can generate more intense precipitation due to a stronger accretion process, in which drizzle drops grow by collecting small cloud drops and other drizzle drops lying in the fall path.

In addition to the MBL cloud microphysical properties, the macrophysical properties also play an important role in MBL cloud and precipitation processes. MBL clouds often form in subsident regions and are maintained mainly through the turbulence generated by cloud-top longwave cooling (Wood 2012; Dong et al. 2014a). As the cloud layer becomes deeper, the turbulence can no longer sustain the mixing down to the surface. Subsequently, the cloud layer becomes decoupled from the surface and exhibits different properties from the clouds in a coupled MBL (Jones et al. 2011; Dong et al. 2015). The optical properties of MBL clouds also depend on both the microphysics and macrophysics. It is thus imperative to provide long-term observations and retrievals to constrain model simulations.

[a] Current affiliation: Pacific Northwest National Laboratory, Richland, Washington.

Corresponding author: Dr. Xiquan Dong, xdong@email.arizona.edu

DOI: 10.1175/JCLI-D-20-0272.1

TABLE 1. Cloud and drizzle properties derived from ground-based measurements and retrievals.

Cloud/drizzle parameter	Instrument/method	Uncertainty	Reference
Cloud-base height	Ceilometer/micropulse lidar	15 m/30 m	Clothiaux et al. (2000); Morris (2016); Rémillard et al. (2012)
Cloud-top height	Ka-band ARM Cloud Radar	30 m	Kollias et al. (2016); Rémillard et al. (2012)
Drizzle-base height	Ka-band ARM Cloud Radar	30 m	Kollias et al. (2016); Rémillard et al. (2012)
Total liquid water path (TWP)	Three-channel microwave radiometer	$\sim$20 g m^{-2} for TWP $<$ 200 g m^{-2}; $\sim$10% for TWP $>$ 200 g m^{-2}	Turner et al. (2007); Cadeddu et al. (2013, 2017); Liljegren et al. (2001); Dong et al. (2000)
Cloud properties: r_c, N_c, LWC$_c$	Ground-based retrieval	15% for r_c, 35% for N_c, and 30% for LWC$_c$	Wu et al. (2020)
Drizzle properties: r_d, N_d, LWC$_d$	Ground-based retrieval	30% for r_d, 50% for N_d and LWC$_d$	Wu et al. (2020)

To provide much needed observations, the Clouds, Aerosol, and Precipitation in the Marine Boundary Layer (CAP-MBL) field campaign was conducted by deploying the Department of Energy Atmospheric Radiation Measurement (ARM) Mobile Facility (AMF) in Graciosa Island, Azores, in the eastern Atlantic from April 2009 to December 2010 (Wood et al. 2015). The Azores island chain is located at the boundary of the subtropics and the midlatitudes, and is thus subject to a wide range of meteorological conditions with high pressure systems dominating in summer whereas low pressure systems are dominant in winter (Dong et al. 2014a; Wood et al. 2015). The monthly mean MBL cloud fraction (CF) during CAP-MBL ranged from 20% to 40%, which correlates well with the prevailing synoptic patterns with a maximum frequency of occurrence in summer and minimum in winter (Rémillard et al. 2012; Dong et al. 2014a). The MBL clouds frequently precipitated over the Azores, most of which were in the form of virga (Rémillard et al. 2012; Wu et al. 2015).

Dong et al. (2014a,b, hereafter D14a and D14b) investigated the seasonal and diurnal variations of MBL CFs, cloud macro- and microphysical properties, and surface cloud condensation nuclei (CCN) measurements during CAP-MBL using ground-based observations and retrievals. The MBL cloud layers, in general, were lower, warmer, and thinner with larger total liquid water path (TWP) and LWC during summer than those during winter. There were no strong diurnal variations in r_c and N_c. The LWC$_c$ was greater during spring and summer than during autumn and winter, and the nighttime values were greater than the daytime ones, while N_c mainly follow the variations of LWC$_c$. The above-mentioned work advanced our understanding of the controlling parameters in MBL cloud development (e.g., Dong et al. 2015; Wu et al. 2017) and the generated dataset was long enough to evaluate model parameterizations (e.g., Wu et al. 2018). However, the retrieved MBL cloud microphysical properties from D14a and D14b are the layer-mean microphysics using radiative transfer modeling and power-law based regression methods, which did not separate cloud and drizzle properties.

To provide the profiles of MBL cloud and drizzle microphysical properties, innovative methods were recently developed to first decompose drizzle and cloud reflectivity in MBL clouds from ARM cloud radar reflectivity measurements, and then simultaneously retrieve both cloud and drizzle microphysical properties (Wu et al. 2020). These retrieved microphysical properties have been validated by aircraft in situ measurements during Aerosol and Cloud Experiments in the Eastern North Atlantic (ACE-ENA; $\sim$158 h of aircraft data). The retrieval methods were then implemented to all ground-based observations at the ARM ENA site during the period July 2015–September 2019, which provides the long-term observations and retrievals for this study. The manuscript is organized as follows: section 2 describes the dataset and methodology and section 3 presents the results and discussions, followed by summary and conclusions in section 4.

2. Data and method

The ground-based observations were collected at the DOE ARM eastern North Atlantic (ENA) site from July 2015 to September 2019 when all the instruments were functioning. The ARM ENA site is a fixed site that is located within a kilometer of the former CAP-MBL ARM mobile facility (AMF) deployment site. Table 1 lists the cloud and drizzle observations, retrieval methods, their uncertainties, and references.

Cloud and drizzle macrophysical properties, such as CF, cloud-top and cloud-base height (ZT and ZB), and drizzle base height, were taken from cloud radar, lidar, and ceilometer measurements. Cloud thickness (ΔZ_{cld}) is defined as the difference between ZT and ZB. The drizzle base (DB) is defined as the lowest range gate height in radar reflectivity that is greater than -40 dBZ in drizzling periods and the drizzle thickness below the cloud base (ΔZ_{drz}) is the difference between ZB and DB. All other macrophysical properties were derived using the same methods as in D14a. The total liquid water path (TWP) was retrieved from a three-channel microwave radiometer using a physically based method (Turner et al. 2007; Cadeddu et al. 2013, 2017). Cloud and drizzle microphysical properties, such as cloud and drizzle particle sizes (r_c and r_d), number concentrations (N_c and N_d), and liquid water contents (LWC$_c$ and LWC$_d$) were retrieved using the Ka-band ARM Zenith Radar (KAZR), ceilometer (CEIL), and microwave radiometer (MWR) by assuming a lognormal distribution for cloud droplet size distribution (DSD) and normalized gamma distribution for drizzle DSD (Wu et al. 2020). The retrieval started with decomposing KAZR reflectivity into cloud and drizzle reflectivities. Drizzle properties were retrieved first and thus drizzle liquid water path (LWP_d). LWC_c was then retrieved from cloud reflectivity and liquid water path (LWP_c), which was the difference between TWP and LWP_d. The retrievals were validated with collocated aircraft in situ measurements during the Aerosol and Cloud Experiments in the Eastern North Atlantic (ACE-ENA) field campaign in summer 2017 and winter 2018. Both time series and vertical profiles, as well as the statistics from the retrievals agree well with in situ observations (Wu et al. 2020). Treating the aircraft measurements as cloud truth, the median retrieval uncertainties were estimated as ~15% for r_c, ~35% for N_c, ~30% for LWC_c and r_d, and ~50% for N_d and LWC_d. To examine the vertical variations in cloud and drizzle properties, the retrieved microphysics profiles will be shown in normalized height: $z_i = (z - z_{\mathrm{base}})/(z_{\mathrm{top}} - z_{\mathrm{base}})$, where z is the in-cloud height, with cloud base as 0, cloud top as 1, and drizzle base as −1.

Considering an adiabatic assumption, the cloud liquid water content, $\mathrm{LWC}_{\mathrm{ad}}$, increases linearly with height. Here $\mathrm{LWC}_{\mathrm{ad}}$ was calculated by $\mathrm{LWC}_{\mathrm{ad}}(z) = \Gamma_{\mathrm{ad}}(z - zb)$, where $\Gamma_{\mathrm{ad}}(T, p)$ is the adiabatic increase in LWC_c with height, and is a weak function of temperature and pressure (Wood 2005). Most of the observed or retrieved LWC_c values do not follow adiabatic growth and are considered subadiabatic MBL clouds. The reasons for the decrease in adiabaticity ($f_{\mathrm{ad}} = \mathrm{LW}_c/\mathrm{LWC}_{\mathrm{ad}}$) could be a result of drizzle coalescence scavenging (Stevens et al. 1998; Wood 2005; Braun et al. 2018) or cloud-top entrainment (Wood 2012; Yum et al. 2015; Braun et al. 2018). In this study, $\mathrm{LWC}_{\mathrm{ad}}$ values were calculated from interpolated sounding data that have a vertical resolution of 20 m, and the profiles of f_{ad} were classified under three subsets MBL cloud conditions.

The spatial scale of mesoscale convective cellular (MCC) structures in MBL clouds is in the range of 4–30 km (Miller et al. 1995), which cannot be resolved in most of the general circulation models (GCMs). To account for the subgrid variabilities in cloud and drizzle microphysics in GCMs, one approach includes the so-called enhancement factors, which are calculated from the homogeneity parameter $\nu = (\bar{x}/\sigma)^2$, where $\bar{x}$ and σ represent the mean and standard deviation of a variable (e.g., Lebsock et al. 2013). Note that ν depends on the distributions of microphysics in a model grid box. In this study, ν values were calculated using the method of Wu et al. (2018), that is, using the temporal averages of surface retrievals to mimic the spatial averages of model grid size. From its definition, large ν values indicate more homogeneous MBL clouds while small values represent less homogeneous.

To investigate the cloud and drizzle properties under different drizzling status, we further classified the single-layered MBL clouds into three subsets: nondrizzling, virga, and rain clouds. As in Wu et al. (2015, 2020), the cloud was labeled as drizzling if the reflectivity at the cloud base was greater than −37 dBZ. The cloud was labeled as virga if drizzle drops fell out the cloud base but evaporated before reaching the surface, while it was classified as rain period if drizzle drops reached the lowest KAZR range gate. Note that the lowest KAZR range gate is ~160 m above the surface and this may cause uncertainty in the rain period classification and thus ΔZ_{drz} in rain period. Similar to D14a and D14b, the observations and retrievals in this study were averaged into a 5-min resolution. During the 51-month study period (July 2015–September 2019), a total 7644 h of cloud profiles and 4251 h of drizzle profiles were selected to investigate their statistics. As in D14a and D14b, the nighttime was defined as the solar zenith angle greater than 82.5° and daytime less than or equals to 82.5°.

For quantities with no vertical profiles (e.g., ZB, ZT, ΔZ_{cld}, ΔZ_{drz}, TWP, and N_c), the monthly means were simply the averages of the values in the specific months. For example, the average of all the values of single-layered MBL cloud ZB in Januaries was the monthly mean of ZB in January in this study. For quantities with vertical profiles (e.g., LWC_c, r_c, LWC_d, r_d, and N_d), the layer-mean values were first calculated and then to derive their monthly mean values.

3. Results and discussion

We first show the diurnal and seasonal variations of CF, then cloud and drizzle macrophysical and microphysical properties, followed by the adiabaticity and homogeneity parameters. For direct comparisons with the results during CAP-MBL (e.g., D14a; D14b; Rémillard et al. 2012), we also include the statistics for all single-layered MBL clouds, in addition to showing the results for the three subsets (nondrizzling, virga, and rain).

a. Cloud fraction

Monthly means of single-layered MBL cloud fraction (CF_L), and fractions of nondrizzling (CF_N), virga (CF_V), and rain (CF_R) cloud fractions during the 51-month period are shown in Fig. 1. CF_L (black bars in Fig. 1) peaks in July when high pressure systems dominate the Azores (Dong et al. 2014a; Wood et al. 2015). CF_L is at a minimum in December when low pressure systems dominate, with an annual mean of 0.259.

For nondrizzling clouds, CF_N (green bars in Fig. 1) increased from spring to summer and reached the maximum in July, then gradually decreased during the autumn and winter with an annual mean of 0.115, which is 44.4% of all single-layered CF_L. In other words, 55.6% of the single-layered MBL clouds produced precipitation. The precipitating frequency in low-level clouds (summation of green and red bars divided by black in Fig. 1) was higher from late fall to early spring than the period April–September, partially because the dominant low pressure systems generate relatively stronger upward motions that can transport moisture from the surface to the cloud layer. Another reason could be the lower environmental aerosol and CCN number concentrations (N_a and N_{CCN}) during the cool months (D14a; D14b; Wood et al. 2015), which limits N_c and increases precipitation efficiency. The drizzling frequencies (CF_V + CF_R) during the warm months (~45%) were much lower than those during the cool months (>70%), but nearly half of the drizzle events during the summer can reach the surface as liquid precipitation. CF_R values (red bars in Fig. 1) were higher in June, July, and November than in other months.

Figure 2 shows the hourly means of CF_L, CF_N, CF_V, and CF_R. No strong diurnal variations were found in all cloud

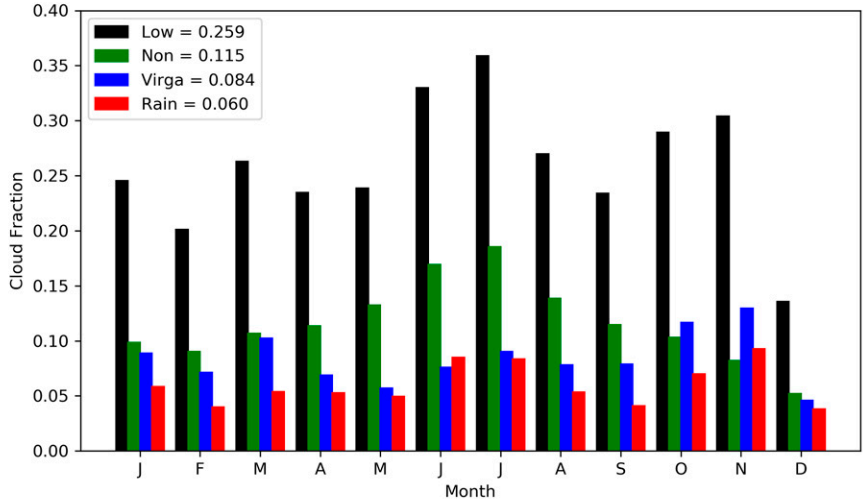

FIG. 1. Monthly mean low cloud (cloud-top height ≤ 3 km) fractions (CFs) derived from DOE ARM radar/lidar measurements during July 2015–September 2019 at the eastern North Atlantic (ENA) site. According to their precipitating status, all single-layered MBL clouds (black) were classified into three categories: nondrizzling (green), virga (drizzle drops evaporate before reaching the surface; blue), and rain (drizzle drops reach the surface; red). The numbers show the average CFs for each category during the study period.

categories. The maximum CF_L occurred during night and morning whereas minimum values were observed in the afternoon, primarily due to the diurnal difference in turbulent mixing generated by cloud-top longwave cooling. During the day, the absorption of solar radiation partially offsets the longwave cooling and reduces the turbulent strength, resulting in the cloud layer being decoupled from surface moisture supply which thus decreases the cloud fraction (Wood 2012; Dong et al. 2015). During the night, the turbulent mixing is not suppressed by the shortwave heating, which favors MBL cloud formation. The CF_N generally followed the variations of CF_L, with slightly higher CFs during the night. CF_V and CF_R also showed minimum values in the afternoon, but the maximum values appeared later than the CF_L peak in the morning, with CF_V maxima in the morning and noon when the cloud layers were thicker.

The results in Fig. 1 are comparable with those in D14a with slight differences in annual and monthly means. The values in Fig. 1 are lower than those in Rémillard et al. (2012, their Fig. 3b) because the low-level clouds in this study were single-layered while all cloudy conditions were considered in Rémillard et al. (2012). Similarly, during the CAP-MBL campaign (D14a; Wood

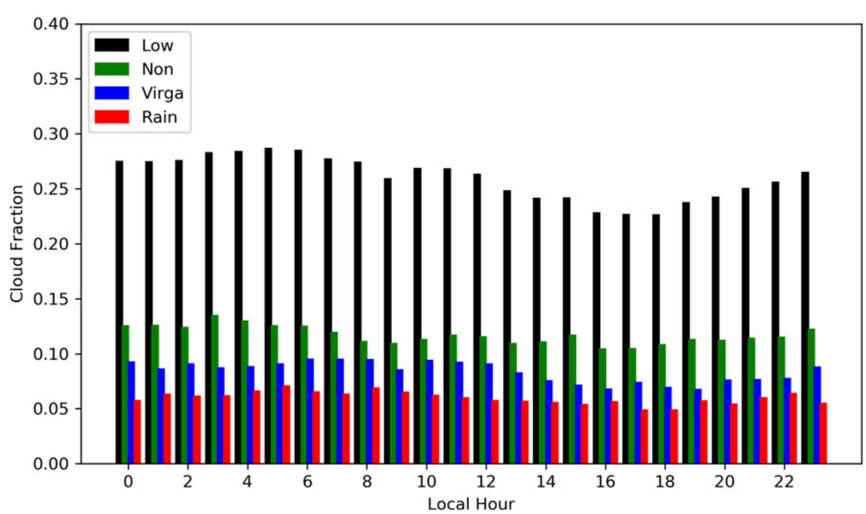

FIG. 2. As in Fig. 1, but for hourly mean single-layered MBL CFs and three categories of CFs. Local time is UTC − 1 h.

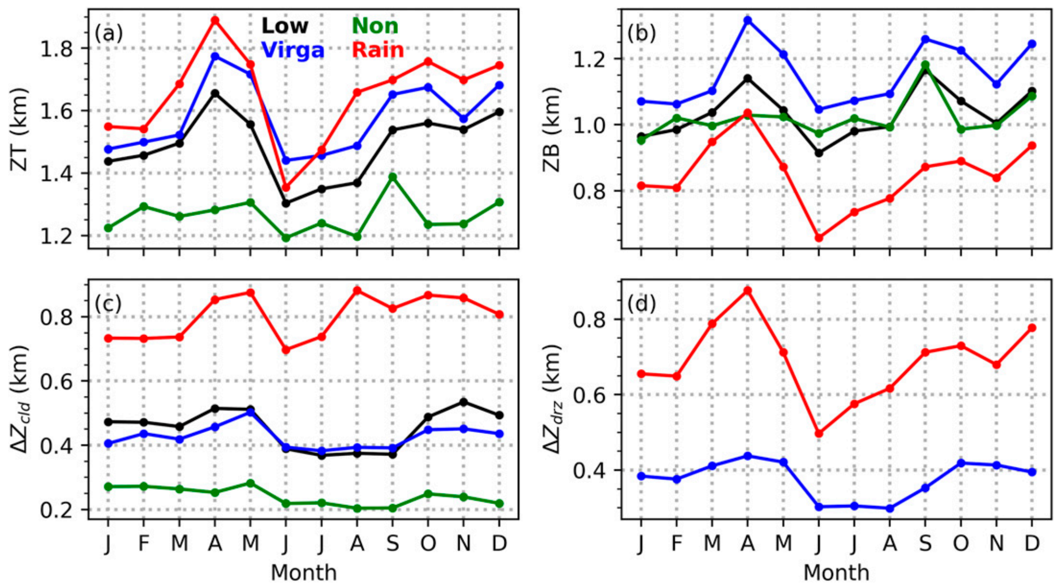

FIG. 3. Monthly means of cloud and drizzle macrophysical properties: (a) cloud-top height (ZT), (b) cloud-base height (ZB), (c) cloud thickness (ΔZ_{cld}), and (d) drizzle virga thickness below the cloud base (ΔZ_{drz}). The colors represent all single-layered MBL clouds (black), nondrizzling clouds (green), virga (blue), and rain (red) clouds.

et al. 2015), there were no strong diurnal variations of MBL clouds at the Azores.

b. *Macrophysical properties*

The seasonal variations of cloud and drizzle macrophysical properties are shown in Fig. 3, with their probability distribution functions (PDFs) shown in Fig. 4 with the same color code as in Fig. 1. The diurnal variations of cloud macrophysical properties are similar to those in D14a and D14b (not shown). The means and standard deviations of the seasonal and diurnal cloud and drizzle macrophysical properties are listed in Table 2.

The cloud-top and cloud-base heights (ZT and ZB) for all categories (except for nondrizzling) reached their maxima in April followed by a significant decrease in May and June, then gradually increased and remained relatively high and invariant from September through December (Figs. 3a,b). Figures 3 and 4 illustrate that rain clouds had the highest ZT (1.64 km) and the lowest ZB (0.84 km), resulting in the deepest cloud layer (0.80 km) among all categories. On the other hand, nondrizzling clouds had the lowest ZT (1.25 km) and ZB of 1.02 km, resulting in the thinnest cloud layer (0.23 km). The PDFs of ZTs and ZBs for nondrizzling, virga, and rain clouds are similar to each other with nearly normal distributions but slightly different peaks (Figs. 4a,b). The cloud thicknesses of rain clouds had the broadest distribution with positive skewness toward thicker cloud layers (Fig. 4c). The seasonal variations in ZB and ZT in this study are in general agreement with those in D14a, except that the values of ZT and ZB are higher in December in this study. The diurnal variations of cloud macrophysical properties are similar to those in D14a and D14b. The seasonal and annual means and standard deviations for all cloud categories are summarized in Table 2.

Figure 3d shows the seasonal variations of drizzle thickness below the cloud base (ΔZ_{drz}) during virga and rain periods, where they both were at a maximum in April, reached a minimum value in June, and then gradually increased toward December. The annual mean of ΔZ_{drz} for virga clouds was 0.42 km with a range of monthly means from 0.2 to 0.4 km, while the annual mean for rain clouds was 0.8 km with a dip of 0.5 km in June and a peak of 0.86 km in April. From Student's t test, there were no significant day–night differences in ΔZ_{drz} for the rain period (p value = 0.7169), but for the virga period, ΔZ_{drz} during night were significantly greater than those during the day (p value = 0.0061). Similar to the PDFs of cloud thickness, the PDF of ΔZ_{drz} during the rain period covered a broader range than the virga period (Fig. 4d). Note that ΔZ_{drz} has been found to depend on the subcloud relative humidity and ΔZ_{cld}, and is an important parameter to determine the air–sea energy and mass exchange in GCMs. Yang et al. (2018) proposed a third-order power-law relationship between cloud and drizzle thickness ($\Delta Z_{\mathrm{drz}} \sim \Delta Z_{\mathrm{cld}}^3$), which shows good agreement with the observations. This relationship fits well with the monthly data in Fig. 4 for the virga periods with a correlation coefficient of 0.77 between ΔZ_{drz} and $\Delta Z_{\mathrm{cld}}^3$, and a relatively lower correlation coefficient of 0.43 for the rain periods, probably because drizzle was intercepted by the surface before it totally evaporated.

c. *Microphysical properties*

Monthly means of cloud and drizzle microphysical properties, such as TWP, LWC_c, r_c, N_c, LWC_d, r_d, and N_d, are shown in Fig. 5. Their corresponding PDFs are presented in Fig. 6 and their seasonal and annual means and standard deviations are listed in Table 3. The cloud microphysical properties should not be compared directly with those presented in D14a and

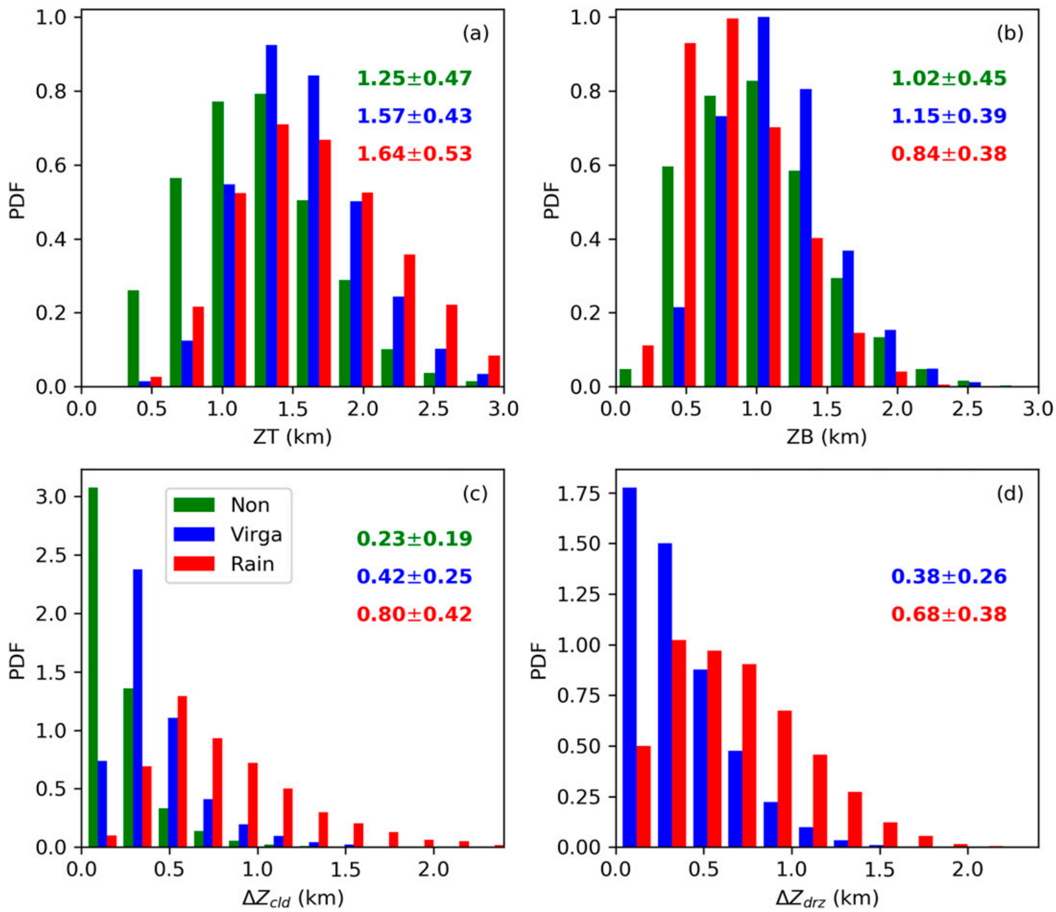

FIG. 4. Probability distribution functions (PDFs) for (a) cloud-top height (ZT), (b) cloud-base height (ZB), (c) cloud thickness (ΔZ_{cld}), and (d) drizzle virga thickness blow the cloud base (ΔZ_{drz}). Colors represent nondrizzling (green), virga (blue), and rain (red) clouds. The means and standard deviations of parameters for each category are indicated in each panel.

D14b because the retrieval algorithm in this study allows to get the cloud and drizzle microphysical properties separately, while in D14a and D14b, the microphysical properties include combined information from cloud and drizzle.

Figure 5a presents the monthly means of TWP for all single-layered MBL clouds and their three subsets. The TWP means were similar to their ΔZ_{cld} counterparts (Fig. 3c) with the largest TWPs found in rain clouds, and the least TWPs were observed in nondrizzling clouds, while the TWPs for virga clouds were similar to those for all single-layered MBL clouds. There were no strong seasonal variations in TWP for all categories. TWPs for rain clouds had minor variations with minima (~200 g m^{-2}) in February and June, and maxima (~250 g m^{-2}) in April and October, which were well correlated with their corresponding ΔZ_{cld} and ΔZ_{drz} values presented in Figs. 3c and 3d. The PDFs of TWP for rain clouds had the broadest distributions, covering a range of 70–700 g m^{-2} (Fig. 6a), while most of the TWP values for nondrizzling clouds were less than 200 g m^{-2}. The annual mean of TWP for rain clouds (236 g m^{-2}) was about 4 times higher than the mean for nondrizzling clouds (59 g m^{-2}), and 2 times higher than the mean for single-layered MBL clouds (115 g m^{-2}).

LWC$_c$ exhibited decreases in May and increases from July to September. Monthly means of LWC$_c$ for rain clouds were much higher than the other three categories (all single-layered MBL cloud, nondrizzling, and virga clouds) with minor seasonal variation, while the monthly means of LWC$_c$ from the other three categories were similar to each other and had relatively large variations. The annual means of LWC$_c$ were 0.20, 0.17, and 0.23 g m^{-3}, respectively, for nondrizzling, virga, and rain clouds. Compared to the large differences in TWP, the slight differences in LWC$_c$ between nondrizzling, virga, and rain clouds primarily resulted from their cloud thickness differences as shown in Fig. 4c. The LWC$_c$ values (Fig. 6b) for nondrizzling clouds were slightly higher than those for virga clouds, which may be due to lack of drizzle initiation mechanisms in nondrizzling clouds. For virga clouds, coalescence scavenging decreases LWC$_c$.

Monthly means of r_c were nearly constant and fluctuated within 1 μm for all cloud categories (Fig. 5c), with rain clouds having the largest mean value while nondrizzling clouds had

TABLE 2. Seasonal and yearly averages of cloud and drizzle macrophysical properties. Numbers in the parenthesis are the standard deviations.

	Winter (day)	Winter (night)	Spring (day)	Spring (night)	Summer (day)	Summer (night)	Autumn (day)	Autumn (night)	Year (day)	Year (night)
					ZB (km)					
Low	0.97 (0.40)	1.03 (0.44)	1.06(0.41)	1.08 (0.41)	0.97 (0.43)	0.96 (0.43)	1.05 (0.42)	1.09 (0.44)	1.01 (0.42)	1.04 (0.44)
Non	0.93 (0.42)	1.05 (0.49)	0.99(0.40)	1.04 (0.42)	1.00 (0.44)	0.99 (0.45)	1.03 (0.46)	1.10 (0.50)	1.00 (0.43)	1.04 (0.47)
Virga	1.10 (0.37)	1.12 (0.41)	1.19(0.37)	1.20 (0.39)	1.10 (0.41)	1.05 (0.40)	1.19 (0.38)	1.21 (0.38)	1.14 (0.39)	1.15 (0.40)
Rain	0.81 (0.35)	0.87 (0.38)	0.96(0.42)	0.95 (0.40)	0.72 (0.35)	0.71 (0.32)	0.84 (0.36)	0.87 (0.37)	0.82 (0.38)	0.85 (0.38)
					ZT (km)					
Low	1.44 (0.48)	1.51 (0.51)	1.56 (0.52)	1.56 (0.51)	1.36 (0.47)	1.33 (0.47)	1.53 (0.49)	1.55 (0.49)	1.45 (0.50)	1.48 (0.50)
Non	1.19 (0.45)	1.30 (0.51)	1.28 (0.44)	1.29 (0.44)	1.23 (0.46)	1.20 (0.46)	1.27 (0.47)	1.32 (0.51)	1.24 (0.46)	1.26 (0.48)
Virga	1.52 (0.42)	1.54(0.44)	1.64 (0.43)	1.65 (0.45)	1.48 (0.42)	1.45 (0.42)	1.62 (0.42)	1.64 (0.41)	1.56 (0.43)	1.57 (0.43)
Rain	1.53 (0.50)	1.64(0.54)	1.78 (0.57)	1.77 (0.55)	1.48 (0.50)	1.47 (0.48)	1.72 (0.50)	1.72 (0.48)	1.62 (0.53)	1.65 (0.52)
					ΔZ_{cld} (km)					
Low	0.47 (0.33)	0.48 (0.35)	0.50 (0.37)	0.49 (0.35)	0.38 (0.34)	0.37 (0.33)	0.48 (0.39)	0.46 (0.36)	0.44 (0.36)	0.44 (0.35)
Non	0.26 (0.20)	0.25 (0.18)	0.29 (0.21)	0.25 (0.16)	0.22 (0.20)	0.21 (0.18)	0.24 (0.21)	0.22 (0.18)	0.24 (0.20)	0.22 (0.17)
Virga	0.42 (0.23)	0.42 (0.23)	0.45 (0.26)	0.45 (0.24)	0.39 (0.25)	0.39 (0.25)	0.44 (0.26)	0.43 (0.25)	0.42 (0.26)	0.42 (0.24)
Rain	0.72 (0.38)	0.77 (0.41)	0.83 (0.44)	0.82 (0.40)	0.76 (0.43)	0.76 (0.40)	0.87 (0.44)	0.84 (0.41)	0.80 (0.43)	0.80 (0.41)
					ΔZ_{drz} (km)					
Low	0.49 (0.33)	0.52 (0.36)	0.56 (0.39)	0.59 (0.38)	0.41 (0.31)	0.41 (0.29)	0.49 (0.34)	0.52 (0.35)	0.48 (0.34)	0.51 (0.35)
Virga	0.38 (0.25)	0.39 (0.27)	0.41 (0.27)	0.44 (0.29)	0.30 (0.22)	0.32 (0.23)	0.38 (0.26)	0.41 (0.28)	0.36 (0.25)	0.39 (0.27)
Rain	0.65 (0.35)	0.71 (0.38)	0.80 (0.42)	0.79 (0.40)	0.56 (0.35)	0.55 (0.32)	0.68 (0.36)	0.71 (0.37)	0.66 (0.38)	0.69 (0.38)

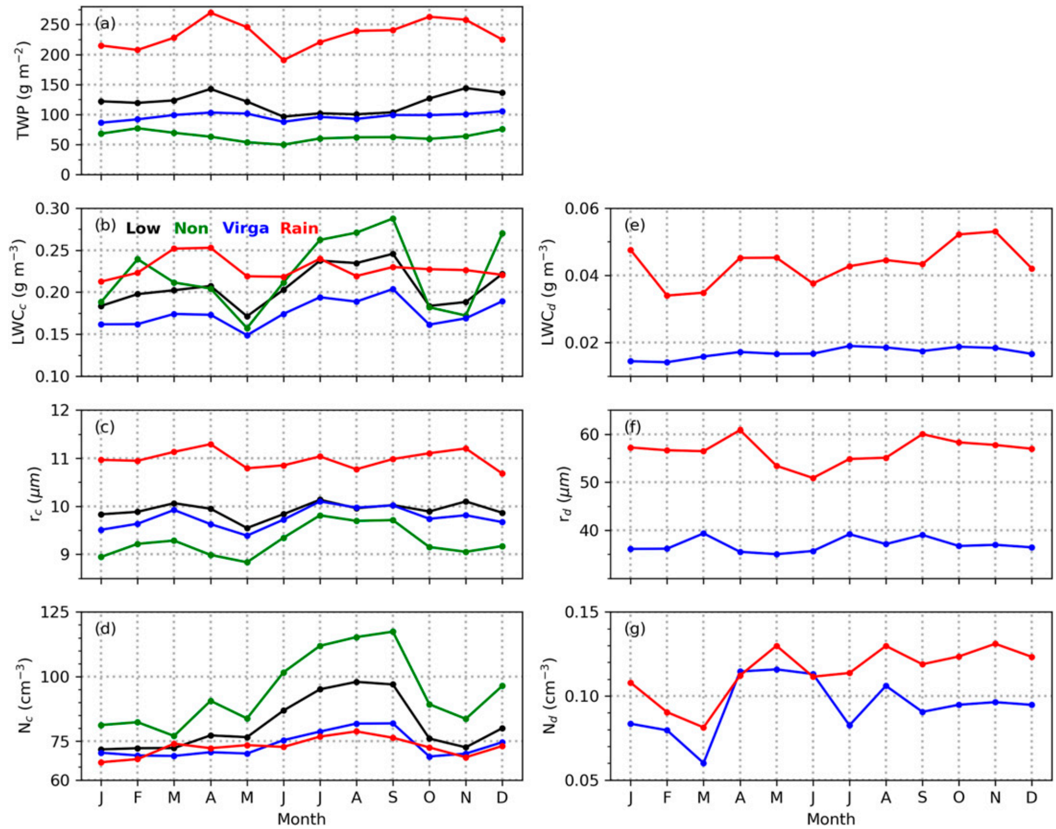

FIG. 5. As in Fig. 3, but for microphysical properties: (a) total liquid water path (TLWP), (b) cloud liquid water content (LWC$_c$), (c) cloud-droplet effective radius (r_c), (d) cloud-droplet number concentration (N_c), (e) drizzle liquid water content (LWC$_d$), (f) drizzle median radius (r_d), and (g) drizzle number concentration (N_d).

the smallest. Table 3 lists the seasonal and annual means of r_c for all categories, as well as their day and night results. In general, the r_c values during the night are slightly greater than those during the day, similar to TWP and LWC$_c$. For nondrizzling and virga clouds, r_c distributions were close to normal with slight skewness to the right (Fig. 6c). The mode value during the rain period (12 μm) was greater than the mean value (11 μm) and the distribution was skewed to the left. The monthly means of N_c basically followed the variations of LWC$_c$, with annual means of 99, 74, and 72 cm^{-3}, respectively, for nondrizzling, virga, and rain clouds.

The seasonal and diurnal variations in r_c are consistent with the findings in D14a and D14b, except that the values are smaller in this study, because D14a and D14b retrieved the layer-mean r_c using solar transmission and power law fitting, which included mixed information on cloud and drizzle sizes whereas in this study, cloud and drizzle values were retrieved separately. The seasonal variations of N_c are consistent with those in D14a and D14b and in Wood et al. (2015) where N_c values were higher in summer and autumn than those in spring and winter, presumably due to high surface CCN number concentrations (D14a; D14b; Wood et al. 2015).

For the retrieved drizzle microphysical properties, the seasonal variations are presented in Figs. 5e–g and the means and standard deviations are listed in Table 3, and no significant seasonal and day–night variations for drizzle microphysical properties were found from this study. The annual means of LWC$_d$ were 0.017 and 0.045 g m^{-3}, respectively, for virga and rain clouds, which were an order of magnitude lower than the LWC$_c$ counterparts. The corresponding N_d means were 0.094 and 0.117 cm^{-3} (three orders of magnitude lower than the N_c counterparts), which resulted in much lower LWC$_d$. The PDFs of r_d (Fig. 6f), especially for rain clouds, were positively skewed which resulted in much larger mean and standard deviation values (56 $\pm$ 34 μm) than those for virga clouds (37 $\pm$ 15 μm).

To investigate the vertical distributions of the retrieved cloud and drizzle microphysical properties, the profiles of cloud and drizzle microphysical properties are height-normalized [$z_i = (z - z_{\rm base})/(z_{\rm top} - z_{\rm base})$, with cloud base as 0, cloud top as 1, and drizzle base as -1] for nondrizzling, virga, and rain clouds in Fig. 7. The retrieved r_c values for all cloud categories, as illustrated in Fig. 7a, monotonically increased from the cloud base until $z_i \approx 0.75$ from condensational growth (Rogers and Yau 1996; Wallace and Hobbs 2006), then decreased toward the cloud top due to cloud-top entrainment. For the range of $z_i = 0.2$–0.9, the r_c values from both virga and rain clouds were much larger than those from nondrizzling clouds due to strong updrafts and deeper cloud layers, while the r_c values were smaller than those from nondrizzling clouds near cloud base.

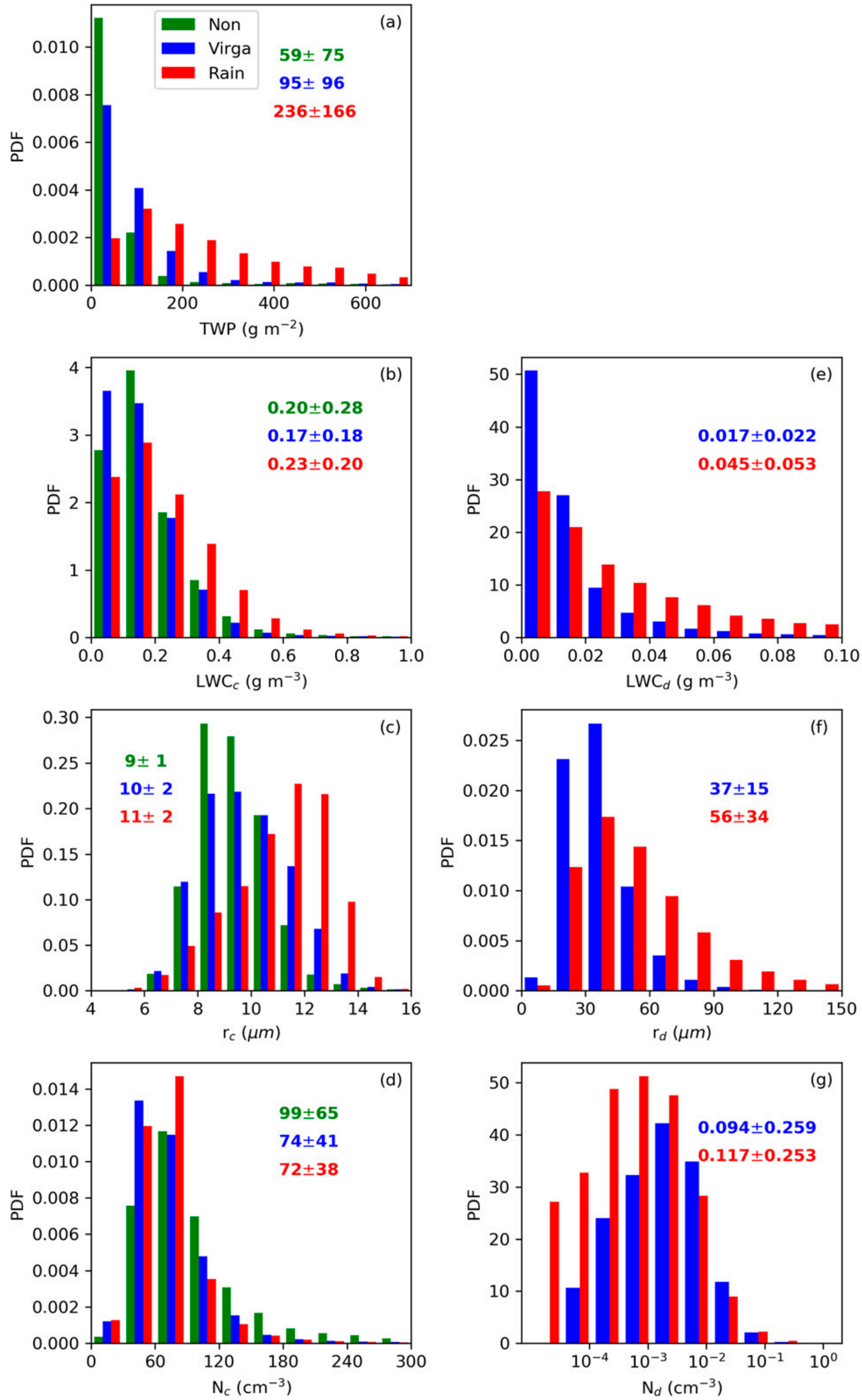

FIG. 6. As in Fig. 4, but for the PDFs of (a) TWP, (b) LWC$_c$, (c) r_c, (d) N_c, (e) LWC$_d$, (f) r_d, and (g) N_d.

TABLE 3. As in Table 2, but for cloud and drizzle microphysical properties.

	Winter (day)	Winter (night)	Spring (day)	Spring (night)	Summer (day)	Summer (night)	Autumn (day)	Autumn (night)	Year (day)	Year (night)
					TWP ($g\,m^{-2}$)					
Low	107.0 (122.2)	127.3 (148.0)	113.8 (133.1)	135.0 (157.5)	95.5 (101.7)	104.9 (114.0)	119.8 (131.6)	127.4 (140.8)	106.8 (119.4)	121.7 (138.1)
Non	50.6 (75.4)	72.3 (119.8)	51.4 (72.3)	64.5 (109.4)	55.6 (53.3)	59.4 (60.4)	59.6 (70.0)	61.4 (77.9)	55.4 (62.6)	62.4 (83.9)
Virga	81.7 (90.5)	93.3 (107.1)	88.4 (96.8)	104.6 (117.4)	86.9 (68.2)	98.5 (86.1)	93.4 (87.4)	101.5 (105.4)	88.4 (84.1)	99.7 (103.8)
Rain	189.8 (148.5)	228.2 (172.5)	228.8 (163.7)	261.3 (180.5)	202.7 (145.8)	234.4 (155.5)	246.8 (169.7)	265.8 (168.9)	218.1 (158.2)	248.8 (169.7)
					LWC_c ($g\,m^{-3}$)					
Low	0.16 (0.18)	0.20 (0.36)	0.16 (0.22)	0.20 (0.29)	0.20 (0.13)	0.23 (0.21)	0.18 (0.18)	0.20 (0.23)	0.18 (0.17)	0.21 (0.26)
Non	0.13 (0.22)	0.24 (0.60)	0.13 (0.16)	0.19 (0.40)	0.21 (0.13)	0.23 (0.24)	0.19 (0.21)	0.21 (0.29)	0.18 (0.17)	0.22 (0.34)
Virga	0.14 (0.16)	0.17 (0.23)	0.14 (0.17)	0.18 (0.21)	0.17 (0.11)	0.20 (0.18)	0.16 (0.16)	0.18 (0.20)	0.16 (0.15)	0.18 (0.21)
Rain	0.20 (0.17)	0.23 (0.20)	0.22 (0.30)	0.26 (0.23)	0.21 (0.16)	0.25 (0.18)	0.20 (0.15)	0.24 (0.18)	0.21 (0.20)	0.24 (0.20)
					r_c (μm)					
Low	9.7 (1.8)	9.8 (1.9)	9.6 (1.8)	10.0 (1.8)	9.9 (1.5)	10.1 (1.5)	9.9 (1.7)	10.0 (1.7)	9.8 (1.6)	10.0 (1.7)
Non	8.7 (1.2)	9.1 (1.6)	8.7 (1.2)	9.2 (1.4)	9.5 (1.3)	9.7 (1.2)	9.2 (1.3)	9.4 (1.3)	9.2 (1.3)	9.5 (1.3)
Virga	9.5 (1.6)	9.5 (1.6)	9.5 (1.6)	9.7 (1.7)	9.9 (1.5)	10.0 (1.5)	9.8 (1.6)	9.8 (1.7)	9.7 (1.6)	9.8 (1.6)
Rain	10.7 (1.9)	10.9 (1.9)	10.8 (1.9)	11.2 (1.8)	10.7 (1.7)	11.2 (1.7)	10.9 (1.8)	11.3 (1.8)	10.8 (1.8)	11.2 (1.8)
					N_c (cm^{-3})					
Low	67.2 (36.7)	76.4 (56.1)	69.7 (40.5)	78.1 (54.8)	89.8 (54.7)	97.8 (60.7)	79.5 (49.7)	82.4 (53.1)	80.5 (49.7)	85.4 (57.1)
Non	71.4 (42.8)	89.0 (81.4)	76.0 (46.5)	87.0 (72.4)	105.5 (60.5)	113.7 (68.0)	98.3 (65.9)	100.4 (66.6)	96.4 (59.9)	102.5 (71.0)
Virga	65.6 (34.7)	73.0 (46.1)	63.6 (33.9)	73.2 (45.3)	74.2 (38.0)	83.5 (46.3)	70.8 (36.8)	74.1 (45.2)	69.7 (36.6)	76.0 (45.9)
Rain	66.0 (33.6)	70.0 (36.2)	70.9 (40.0)	74.6 (40.7)	73.9 (46.2)	78.1 (44.2)	69.7 (34.4)	72.8 (35.4)	70.9 (40.2)	73.9 (39.2)
					LWC_d ($g\,m^{-3}$)					
Virga	0.015 (0.018)	0.014 (0.019)	0.018 (0.023)	0.014 (0.021)	0.020 (0.022)	0.017 (0.021)	0.020 (0.026)	0.017 (0.024)	0.019 (0.023)	0.016 (0.022)
Rain	0.040 (0.050)	0.044 (0.054)	0.041 (0.048)	0.043 (0.050)	0.041 (0.047)	0.042 (0.048)	0.051 (0.059)	0.052 (0.059)	0.043 (0.051)	0.046 (0.054)
					r_d (μm)					
Virga	36.1 (13.8)	36.0 (14.3)	36.8 (15.1)	37.6 (15.5)	37.0 (15.5)	37.9 (16.0)	36.7 (15.8)	37.6 (15.7)	36.7 (15.2)	37.3 (15.5)
Rain	55.3 (32.9)	57.9 (35.2)	55.8 (38.5)	57.9 (36.6)	52.6 (28.4)	54.6 (28.8)	56.7 (36.4)	59.5 (34.9)	54.8 (33.7)	57.6 (34.0)
					N_d (cm^{-3})					
Virga	0.09 (0.26)	0.09 (0.26)	0.11 (0.28)	0.07 (0.21)	0.11 (0.28)	0.09 (0.26)	0.11 (0.29)	0.08 (0.24)	0.11 (0.28)	0.08 (0.24)
Rain	0.11 (0.25)	0.11 (0.23)	0.12 (0.25)	0.10 (0.22)	0.12 (0.27)	0.11 (0.26)	0.14 (0.28)	0.12 (0.24)	0.12 (0.27)	0.11 (0.24)

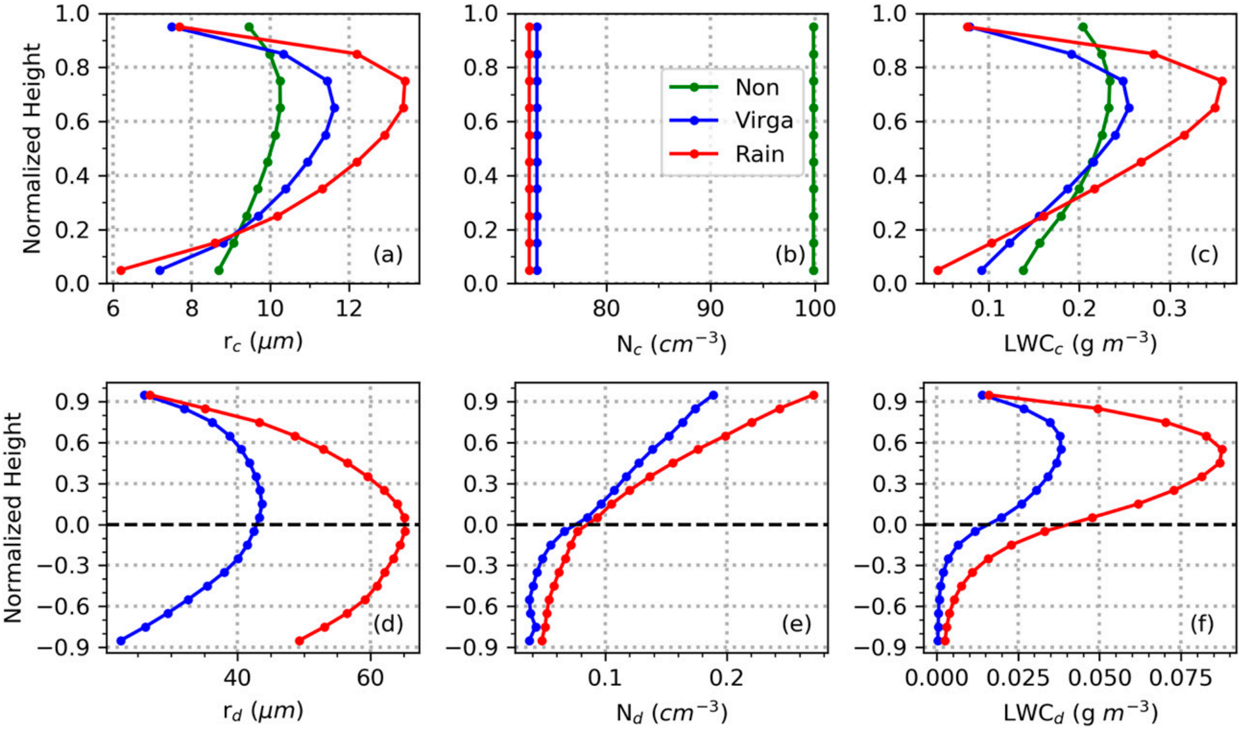

FIG. 7. Profiles of (top) cloud and (bottom) drizzle microphysical properties in normalized height [$z_i = (z - z_{\mathrm{base}})/(z_{\mathrm{top}} - z_{\mathrm{base}})$], with drizzle base as −1, cloud base as 0, and cloud/drizzle top as 1.

There are several explanations for bigger r_c in nondrizzling clouds than those in drizzling clouds near cloud base. The updrafts in nondrizzling clouds are weaker than those in drizzling clouds, and thus the cloud particles near the cloud base could grow larger before the air parcel was lifted farther upward, whereas for drizzling clouds relatively stronger updrafts lifted the cloudy parcels near the cloud base more quickly. Another reason could be the retrieval methods in Wu et al. (2020), where cloud reflectivity at the cloud base was obtained from the difference in radar reflectivity between the range gates above and below the cloud base. This approach is valid if drizzle evaporation can be ignored in the first range gate below the cloud base (~30 m) while drizzle size remains the same. However, collision or breakup of drizzle drops may still happen at the cloud base, which can affect the decomposed cloud reflectivity at the cloud base and thus the retrieved r_c. The smaller r_c values in drizzling clouds near cloud top ($z_i = 0.9$–1) could be due to the large cloud droplets being converted into drizzle drops, thus leaving smaller ones. This could also be an artifact from the constant N_c assumption in the retrieval. Coalescence scavenging near drizzling cloud top leads to less cloud droplets. Using the same N_c as in the middle and lower part of the cloud would result in smaller r_c near the cloud top given a specific LWC$_c$.

Due to the assumption in Wu et al. (2020), the retrieved N_c values remained constant within the cloud and had the largest value for nondrizzling clouds while the N_c values for both virga and rain clouds were nearly the same. The profiles of LWC$_c$ (Fig. 7c), in general, followed the vertical variations of r_c with the largest value at $z_i \approx 0.75$. As demonstrated in Figs. 5b and 6b, the LWC$_c$ values for nondrizzling clouds could be higher than those from drizzling clouds. From the normalized profiles, the LWC$_c$ values for nondrizzling clouds were greater at $z_i = 0$ to 0.3 but much smaller at $z_i = 0.3$ to 0.8 than those for drizzling clouds.

The retrieved r_d values for virga and rain clouds were close to the maximum cloud droplet size (~15 μm) at the cloud top, then increased rapidly toward the cloud base (Fig. 7d). Once drizzle drops fall out of cloud base, their sizes rapidly decrease due to net evaporation. Drizzle drops for rain clouds grew much faster than those for virga clouds, and the averaged r_d at the cloud base (~65 μm) was ~20 μm greater than the virga one. The rapid growth in drizzle drop size for rain clouds could be attributed to the deeper cloud layers (Figs. 3c and 4c) allowing a longer path for drizzle drops to collect other smaller particles. This could also be due to the relatively stronger updraft at the cloud base, which can increase the in-cloud residence time of the drizzle drops, making them grow larger (Feingold et al. 1996).

The retrieved N_d values for both virga and rain clouds decreased dramatically from the cloud top to the cloud base (Fig. 7e), presumably due to self-collection processes. Below the cloud base, the N_d values for virga clouds decreased faster due to quicker evaporation of smaller drops. The distributions of N_d both have strong negative skewness (Fig. 6g), resulting in the mean values smaller than median values. The profiles of median values (not show) had a clearer separation for virga

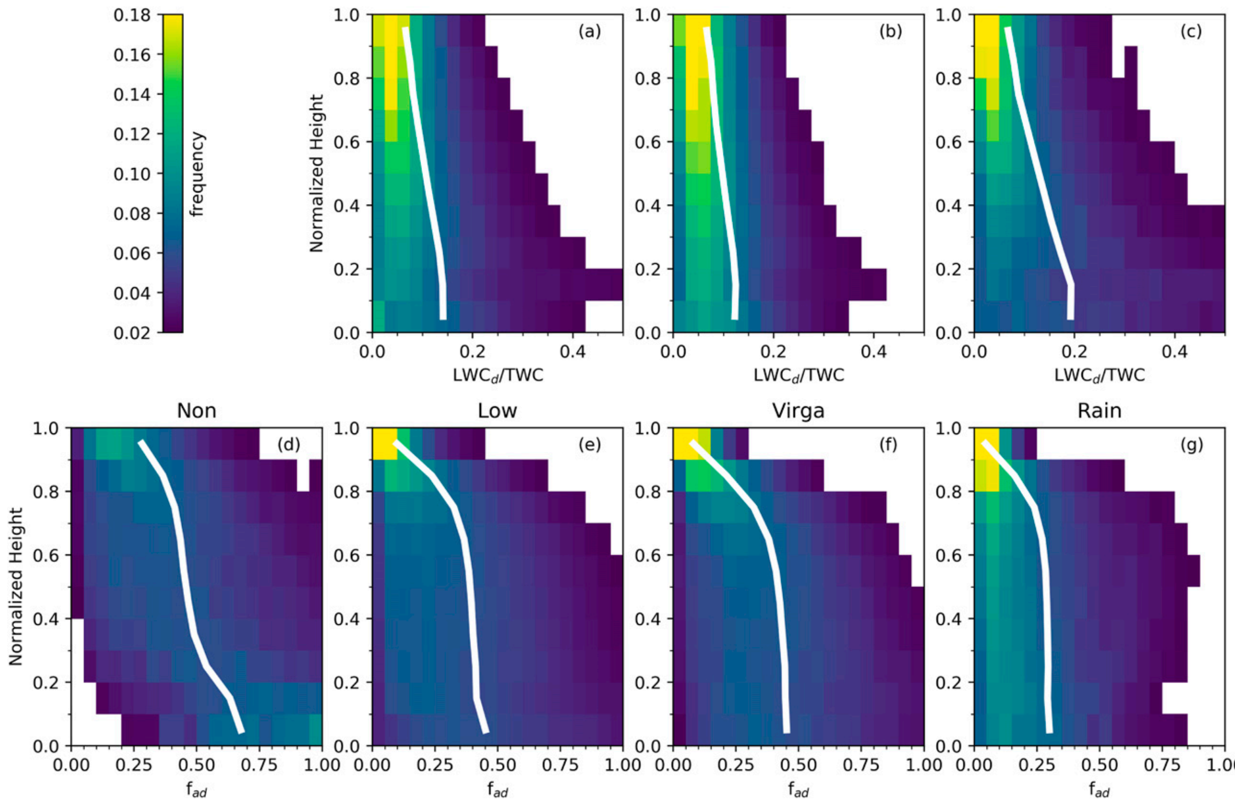

FIG. 8. (top) Frequency distributions of normalized profiles of the ratios of drizzle liquid water content (LWC_d) to total water content (TWC) for (a) all single-layered MBL clouds, (b) virga, and (c) rain MBL clouds. (bottom) Frequency distributions of normalized profiles of the ratios of retrieved cloud LWC_c to calculated LWC_{ad} using an adiabatic method by cloud-base and cloud-top heights ($f_{ad} = LWC_c/LWC_{ad}$) for (d) nonprecipitating, (e) all single-layered, (f) virga, and (g) rain MBL clouds. The white lines represent the median values at each level of normalized height.

and rain periods, especially at the cloud base. For both virga and rain clouds, the LWC_d values increased from the cloud top down to the middle of the cloud ($z_i = 0.5$), where they reached a maximum, and then decreased downward. The LWC_d values for rain clouds were higher than those from virga clouds except at the cloud top, where the rain and virga values were nearly equivalent (Fig. 7f).

d. Adiabaticity and homogeneity

Figures 8a–c show the frequency distributions of normalized profiles of the ratios of LWC_d to TWC ($LWC_c + LWC_d$) for all single-layered MBL clouds (Fig. 8a), virga (Fig. 8b), and rain (Fig. 8c) clouds in normalized height (upper row) and the frequency distributions of normalized profiles of the adiabaticity $f_{ad} = LWC_c/LWC_{ad}$ for the same three categories along with the nondrizzling clouds (bottom row). Figures 8a and 8e represent the distributions for all single-layered MBL clouds at the ENA site and can be used as the mean states in parameterization development and diagnostics over the Azores or northeast Atlantic.

Although the LWC_d profiles for both virga and rain clouds in Fig. 7f showed maximum values in the middle of cloud and decreased toward cloud boundaries, the median ratios of LWC_d to TWC increased from the cloud top to the cloud base, where the ratios were highest (white lines in Figs. 8a–c). The LWC_d ratios for all single-layered and virga clouds were close to each other but both were smaller than those for rain clouds. The median ratios for virga and rain clouds were less than 0.1 near the cloud top, and can be up to 0.4 at the cloud base, suggesting that the LWC_d values at the cloud top or the upper part of the cloud are negligible but their contributions to total liquid water in the lower part of the cloud cannot be ignored.

The adiabaticity f_{ad} values for all subsets monotonically decreased from the cloud base to the cloud top, where they reach the minimum, which is due to, in addition to precipitation scavenging, the mixing of warm, dry air by cloud-top entrainment. The f_{ad} values dramatically increased from $z_i = 1$ to $z_i \approx 0.6$, then remained nearly invariant toward the cloud base except for nondrizzling clouds, suggesting that the cloud-top entrainment mixing can affect as deep as the upper ~40% of the cloud layer. The f_{ad} values were the greatest for nondrizzling clouds (Fig. 8d) with the maximum of ~0.7 at the cloud base, and the smallest for rain clouds (Fig. 8g) with the maximum of ~0.3 at the cloud base. The f_{ad} values for all single-layered (Fig. 8e) and virga (Fig. 8f) clouds fell between nondrizzling (Fig. 8d) and rain (Fig. 8g) clouds. The different

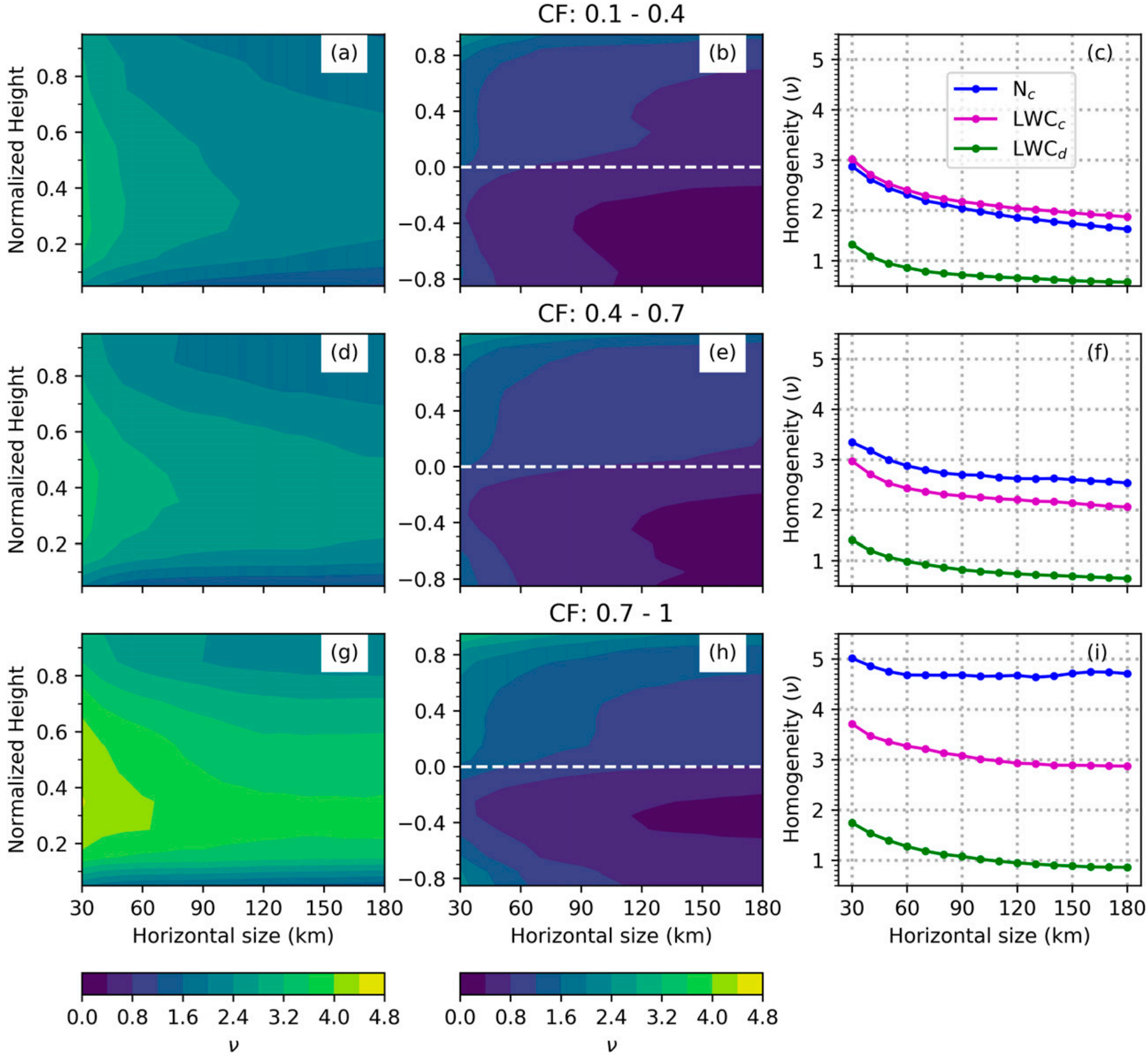

FIG. 9. (left) Profiles of LWC_c homogeneity parameter [$\nu = (\overline{x}/\sigma)^2$, where $\overline{x}$ and σ represent mean and standard deviation of a variable] as functions of horizontal length in normalized height [$z_i = (z - z_{\mathrm{base}})/(z_{\mathrm{top}} - z_{\mathrm{base}})$] and different cloud fraction (CF). (middle) As in the left column, but for LWC_d. The white dashed line denotes the cloud base. (right) ν as a function of horizontal length calculated from layer-mean LWC_c, LWC_d, and N_c.

f_{ad} values between nondrizzling and drizzling clouds indicate that the presence of precipitation, or precipitation scavenging, results in f_{ad} decreased by 0.25 to 0.4, depending on drizzle intensity. These results provide insightful information on model parameterizations of cloud-top entrainment, but further studies are needed about the causes of subadiabaticity for nondrizzling clouds, besides the cloud-top entrainment.

The homogeneity parameter (ν) is often used to account for cloud and precipitation subgrid variabilities when applying microphysical schemes to GCMs (Morrison and Gettelman 2008; Wu et al. 2018; Lebsock et al. 2013; Zhang et al. 2019). Unlike Wu et al. (2018), in which they used the layer-mean microphysics to calculate ν and the enhancement factors, we calculated the profiles of ν in this study. In addition, we separated clouds according to their CF into three categories as shown in Fig. 9 and calculated ν in each category. We also analyzed the dependence of ν on boundary layer stability by separating clouds according to lower tropospheric stability (LTS). It was found that ν increases when the boundary was more stable. However, since the parameterization of subgrid variations is more directly related to CF, we show the dependence of ν on CF below. The left two columns of Fig. 9 show the ν values calculated from LWC_c and LWC_d as functions of different horizontal sampling sizes in normalized height. The horizontal sizes were calculated from the 5-min horizontal wind at cloud level from the interpolated sounding and they were analogs to the model grid sizes. By definition, the larger ν is, the more homogeneous the field is. As shown in the first column, Fig. 9d for example, the LWC_c values were more homogeneous in the middle and lower half of the cloud and in smaller horizontal sizes, but they had relatively large variations near the cloud boundaries. With increased horizontal sizes, LWC_c became increasingly inhomogeneous, which makes sense because clouds over a large domain are likely to have larger variations in the structures, for instance, multiple MCC elements can be sampled. The dependence of ν on height and horizontal size were the same for the three CF categories. With the increase of CF, however, ν became greater, suggesting a more homogeneous LWC_c field.

The LWC_d field was less homogeneous (middle column in Fig. 9) than the LWC_c field due to its intermittency (Wood 2005); similar to LWC_c, LWC_d became less homogeneous with increasing horizontal sizes. The horizontal variations in LWC_d were the smallest near the cloud top and the homogeneity decreased toward the cloud base with the least homogeneity occurred below the cloud base. This structure makes physical sense, because as drizzle drops fall, they grow by the collision–coalescence process, which will result in collections or breakups in the drops and lead to larger variations in the depth of the cloud layer. Changes in ν for LWC_d when CF increases were not as clear as those for LWC_c and the values remain relatively small.

The right column in Fig. 9 shows the ν values calculated from the layer-mean LWC_c, LWC_d, and N_c parameters. The ν values depict the variation of each individual cloud parameter at a range of horizontal sizes. For a given horizontal size, the ν values calculated from N_c were close to those from LWC_c when CF < 0.7, indicating comparable horizontal variability in N_c and LWC_c. When CF $>$ 0.7, the ν values calculated from N_c were much greater than those from LWC_c and the differences across different horizontal sizes became smaller. The term ν is the key parameter used to calculate the subgrid enhancement factors in GCM microphysics parameterizations (Morrison and Gettelman 2008; Wu et al. 2018; Lebsock et al. 2013; Zhang et al. 2019) and very often the subgrid variability in N_c is ignored due to the difficulties or uncertainties in retrieving N_c from satellite observations. The results here suggest that ignoring the variability in N_c could result in large uncertainty in parameterizing the precipitation rate (specifically the autoconversion and accretion rates) in GCMs, especially when CF is low. Using formulas from Lebsock et al. (2013), Wu et al. (2018), and Zhang et al. (2019), an increase of 25%–50% in autoconversion rate was found in the Morrison and Gettelman (2008) scheme by considering the subgrid variations in N_c.

It should be noted, however, that the adiabaticity and homogeneity presented in Figs. 8 and 9 represent the mean conditions over the Azores region, and may not be representative over other climatological regimes, for example, the eastern Pacific. Thus, the results here should serve as local diagnostic benchmark for parameterization development, rather than be used adequately over the globe.

4. Summary and conclusions

This study presents climatology of cloud and drizzle properties over the eastern North Atlantic. More than 4 years of ground-based observations and retrievals were collected, processed, and analyzed at the DOE ARM ENA site from July 2015 to September 2019. The seasonal and diurnal variations in cloud and drizzle macro- and microphysical properties were examined, as well as their vertical and horizontal variations. The seasonal and diurnal variations were compared with the results in D14a,b from the CAP-MBL campaign. Through the analysis, we draw the following conclusions:

1) The single-layered MBL clouds occurred more frequently in summer than in winter, and more frequently during night and morning than the afternoon. The nondrizzling cloud fractions peaked in summer with minima in winter. The annual average drizzling occurrence in all single-layered MBL clouds was ~55% with higher frequency in cold months (>70%) and lower frequency in warm months (~45%). During summer, nearly half of the drizzle events can reach the surface as rain.
2) ZT and ZB were lower during summer than winter, resulted in thinner cloud layers. The rain clouds had the highest ZT (1.64 km) and the lowest ZB (0.84 km), resulted in the deepest cloud layer (0.80 km), while the nondrizzling clouds had the lowest ZT (1.25 km), average ZB (1.02 km), and the thinnest cloud layer (0.23 km). The annual means of $\Delta Z_{\rm drz}$ for virga and rain clouds were 0.42 and 0.8 km, respectively, with significant day–night difference for virga clouds.
3) Similar to the $\Delta Z_{\rm cld}$ counterparts, the TWPs for rain clouds were the largest and for nondrizzling clouds were the least. Seasonal variations of r_c generally followed the variations of LWC_c with larger values in summer than in winter and spring. The r_c values were the largest for rain clouds and the smallest for nondrizzling periods, and the nighttime values were greater than the daytime values. The N_c values were also higher in summer than other seasons and higher during night than during day. The LWC_d, r_d, and N_d were all greater for rain clouds than those for virga clouds with no apparent diurnal differences. The N_d and LWC_d were three orders and one order of magnitude lower, respectively, than their cloud counterparts.
4) The r_c and LWC_c values increased from the cloud base to $z_i \approx 0.75$ by condensational growth, and then decreased toward the cloud top with the largest values for rain clouds due to relatively stronger updrafts. The r_d values increased from the cloud top downward the cloud base from the collision–coalescence process where r_d reached maxima, and then decreased below the cloud base due to net evaporation. Vertical trend of N_d was opposite to r_d due to self-collection. LWC_d maximized in the middle of the cloud and decreased toward the cloud boundaries. However, the fraction of LWC_d in total water content kept increasing from the cloud top to the cloud base where its contribution to total liquid water cannot be ignored.
5) The adiabaticity $f_{\rm ad}$ values monotonically increased from the cloud top to the cloud base with the maxima of ~0.7 for nondrizzling clouds and of 0.3 for rain clouds at the cloud base. At the ENA, drizzling process may decrease $f_{\rm ad}$ by 0.25 to 0.4, and the cloud-top entrainment mixing could significantly impact the upper 20% of the cloud layers, and as deep as the upper 40%. LWC_c was more homogeneous in the middle of the cloud and when the horizontal sampling sizes were smaller. N_c had comparable horizontal variability as LWC_c when CF < 0.7 and should not be ignored in GCM parameterizations. LWC_d

was more homogeneous near cloud top and became less homogeneous toward and below the cloud base and when horizontal sampling sizes were larger. With the increase of CF, LWC_c and N_c became more homogeneous while little changes were found in the LWC_d field.

The above findings provide statistical results about MBL cloud and drizzle properties from the longest record of ground-based observations and retrievals so far over the remote ocean and can serve as baselines for studying MBL cloud-to-rain conversation and growth processes. The 4-yr dataset also provided statistically reliable estimates for the seasonal and diurnal variations in cloud and drizzle properties, which could be useful for evaluating model simulated MBL cloud and precipitation properties or in constraining model parameterizations. However, this study only focused on cloud and drizzle properties themselves and did not include the ambient environmental variables (e.g., temperature, relative humidity, wind speed and direction) and aerosol and CCN information, all of which could be in close relationships with the cloud and drizzle properties presented here and will be investigated and reported in future work.

Acknowledgments. The ground-based measurements were obtained from the Atmospheric Radiation Measurement (ARM) Program sponsored by the U.S. Department of Energy (DOE) Office of Energy Research, Office of Health and Environmental Research, and Environmental Sciences Division. The data can be downloaded from http://www.archive.arm.gov/. This research was supported by the NSF project under Grant AGS-1700728 at the University of Arizona, and also supported as part of the "Enabling Aerosol-cloud interactions at GLobal convection-permitting scalES (EAGLES)" project (74358), funded by the U.S. Department of Energy, Office of Science, Office of Biological and Environmental Research, Earth System Modeling program with the subcontract to the University of Arizona. Mikael Witte and the two anonymous reviewers are acknowledged for their constructive comments.

REFERENCES

Beheng, K. D., 1994: A parameterization of warm cloud microphysical conversion processes. *Atmos. Res.*, **33**, 193–206, https://doi.org/10.1016/0169-8095(94)90020-5.

Bony, S., and J. L. Dufresne, 2005: Marine boundary layer clouds at the heart of tropical cloud feedback uncertainties in climate models. *Geophys. Res. Lett.*, **32**, L20806, https://doi.org/10.1029/2005GL023851.

Braun, R. A., and Coauthors, 2018: Cloud adiabaticity and its relationship to marine stratocumulus characteristics over the northeast Pacific Ocean. *J. Geophys. Res. Atmos.*, **123**, 13 790–13 806, https://doi.org/10.1029/2018JD029287.

Cadeddu, M. P., J. C. Liljegren, and D. D. Turner, 2013: The Atmospheric Radiation Measurement (ARM) program network of microwave radiometers: Instrumentation, data, and retrievals. *Atmos. Meas. Tech.*, **6**, 2359–2372, https://doi.org/10.5194/amt-6-2359-2013.

——, R. Marchand, E. Orlandi, D. D. Turner, and M. Mech, 2017: Microwave passive ground-based retrievals of cloud and rain liquid water path in drizzling clouds: Challenges and possibilities. *IEEE Trans. Geosci. Remote Sens.*, **55**, 6468–6481, https://doi.org/10.1109/TGRS.2017.2728699.

Clothiaux, E. E., T. P. Ackerman, G. G. Mace, K. P. Moran, R. T. Marchand, M. A. Miller, and B. E. Martner, 2000: Objective determination of cloud heights and radar reflectivities using a combination of active remote sensors at the ARM CART sites. *J. Appl. Meteor.*, **39**, 645–665, https://doi.org/10.1175/1520-0450(2000)039<0645:ODOCHA>2.0.CO;2.

Dolinar, E. K., X. Dong, B. Xi, J. H. Jiang, and H. Su, 2015: Evaluation of CMIP5 simulated clouds and TOA radiation budgets using NASA satellite observations. *Climate Dyn.*, **44**, 2229–2247, https://doi.org/10.1007/s00382-014-2158-9.

Dong, X., P. Minnis, T. P. Ackerman, E. E. Clothiaux, G. G. Mace, C. N. Long, and J. C. Liljegren, 2000: A 25-month database of stratus cloud properties generated from ground-based measurements at the Atmospheric Radiation Measurement Southern Great Plains site. *J. Geophys. Res.*, **105**, 4529–4537, https://doi.org/10.1029/1999JD901159.

——, B. Xi, A. Kennedy, P. Minnis, and R. Wood, 2014a: A 19-month record of marine aerosol–cloud–radiation properties derived from DOE ARM mobile facility deployment at the Azores. Part I: Cloud fraction and single-layered MBL cloud properties. *J. Climate*, **27**, 3665–3682, https://doi.org/10.1175/JCLI-D-13-00553.1.

——, ——, P. Wu, X. Dong, B. Xi, and P. Wu, 2014b: Investigation of the diurnal variation of marine boundary layer cloud microphysical properties at the Azores. *J. Climate*, **27**, 8827–8835, https://doi.org/10.1175/JCLI-D-14-00434.1.

——, A. C. Schwantes, B. Xi, and P. Wu, 2015: Investigation of the marine boundary layer cloud and CCN properties under coupled and decoupled conditions over the Azores. *J. Geophys. Res. Atmos.*, **120**, 6179–6191, https://doi.org/10.1002/2014JD022939.

Feingold, G., W. R. Cotton, B. Stevens, A. S. Frisch, G. Feingold, W. R. Cotton, B. Stevens, and A. S. Frisch, 1996: The relationship between drop in-cloud residence time and drizzle production in numerically simulated stratocumulus clouds. *J. Atmos. Sci.*, **53**, 1108–1122, https://doi.org/10.1175/1520-0469(1996)053<1108:TRBDIC>2.0.CO;2.

Jones, C. R., C. S. Bretherton, and D. Leon, 2011: Coupled vs. decoupled boundary layers in VOCALS-REx. *Atmos. Chem. Phys.*, **11**, 7143–7153, https://doi.org/10.5194/acp-11-7143-2011.

Khairoutdinov, M., and Y. Kogan, 2000: A new cloud physics parameterization in a large-eddy simulation model of marine stratocumulus. *Mon. Wea. Rev.*, **128**, 229–243, https://doi.org/10.1175/1520-0493(2000)128<0229:ANCPPI>2.0.CO;2.

Klein, S. A., and D. L. Hartmann, 1993: The seasonal cycle of low stratiform clouds. *J. Climate*, **6**, 1587–1606, https://doi.org/10.1175/1520-0442(1993)006<1587:TSCOLS>2.0.CO;2.

Kollias, P., and Coauthors, 2016: Development and applications of ARM millimeter-wavelength cloud radars. *The Atmospheric Radiation Measurement (ARM) Program: The First 20 Years*, *Meteor. Monogr.*, No. 57, Amer. Meteor. Soc., https://doi.org/10.1175/AMSMONOGRAPHS-D-15-0037.1.

Lebsock, M., H. Morrison, and A. Gettelman, 2013: Microphysical implications of cloud-precipitation covariance derived from satellite remote sensing. *J. Geophys. Res. Atmos.*, **118**, 6521–6533, https://doi.org/10.1002/JGRD.50347.

Liljegren, J. C., E. E. Clothiaux, G. G. Mace, S. Kato, and X. Dong, 2001: A new retrieval for cloud liquid water path using a ground-based microwave radiometer and measurements of cloud temperature. *J. Geophys. Res.*, **106**, 14 485–14 500, https://doi.org/10.1029/2000JD900817.

Liu, Y., and P. H. Daum, 2004: Parameterization of the autoconversion process. Part I: Analytical formulation of the Kessler-type parameterizations. *J. Atmos. Sci.*, **61**, 1539–1548, https://doi.org/10.1175/1520-0469(2004)061<1539:POTAPI>2.0.CO;2.

——, ——, R. McGraw, and R. Wood, 2006: Parameterization of the autoconversion process. Part II: Generalization of Sundqvist-type parameterizations. *J. Atmos. Sci.*, **63**, 1103–1109, https://doi.org/10.1175/JAS3675.1.

——, ——, ——, M. A. Miller, and S. Niu, 2007: Theoretical expression for the autoconversion rate of the cloud droplet number concentration. *Geophys. Res. Lett.*, **34**, L16821, https://doi.org/10.1029/2007GL030389.

Miller, M. A., B. A. Albrecht, M. A. Miller, and B. A. Albrecht, 1995: Surface-based observations of mesoscale cumulus–stratocumulus interaction during ASTEX. *J. Atmos. Sci.*, **52**, 2809–2826, https://doi.org/10.1175/1520-0469(1995)052<2809:SBOOMC>2.0.CO;2.

Morris, V. R., 2016: Ceilometer instrument handbook. Atmospheric Radiation Measurement Rep. ARM SC-ARM-TR-020, 26 pp., https://www.arm.gov/publications/tech_reports/handbooks/ceil_handbook.pdf.

Morrison, H., and A. Gettelman, 2008: A new two-moment bulk stratiform cloud microphysics scheme in the Community Atmosphere Model, version 3 (CAM3). Part I: Description and numerical tests. *J. Climate*, **21**, 3642–3659, https://doi.org/10.1175/2008JCLI2105.1.

Nam, C., S. Bony, J. L. Dufresne, and H. Chepfer, 2012: The too few, too bright tropical low-cloud problem in CMIP5 models. *Geophys. Res. Lett.*, **39**, L21801, https://doi.org/10.1029/2012GL053421.

Randall, D. A., J. A. Coakley, D. H. Lenschow, C. W. Fairall, and R. A. Kropfli, 1984: Outlook for research on subtropical marine stratification clouds. *Bull. Amer. Meteor. Soc.*, **65**, 1290–1301, https://doi.org/10.1175/1520-0477(1984)065<1290:OFROSM>2.0.CO;2.

Rémillard, J., P. Kollias, E. Luke, and R. Wood, 2012: Marine boundary layer cloud observations in the Azores. *J. Climate*, **25**, 7381–7398, https://doi.org/10.1175/JCLI-D-11-00610.1.

Rogers, R. R., and M. K. Yau, 1996: *Short Course in Cloud Physics*. Elsevier, 295 pp.

Slingo, A., 1990: Sensitivity of the Earth's radiation budget to changes in low clouds. *Nature*, **343**, 49–51, https://doi.org/10.1038/343049a0.

Stevens, B., W. R. Cotton, G. Feingold, C.-H. Moeng, B. Stevens, W. R. Cotton, G. Feingold, and C.-H. Moeng, 1998: Large-eddy simulations of strongly precipitating, shallow, stratocumulus-topped boundary layers. *J. Atmos. Sci.*, **55**, 3616–3638, https://doi.org/10.1175/1520-0469(1998)055<3616:LESOSP>2.0.CO;2.

Tripoli, G. J., W. R. Cotton, G. J. Tripoli, and W. R. Cotton, 1980: A numerical investigation of several factors contributing to the observed variable intensity of deep convection over south Florida. *J. Appl. Meteor.*, **19**, 1037–1063, https://doi.org/10.1175/1520-0450(1980)019<1037:ANIOSF>2.0.CO;2.

Turner, D. D., S. A. Clough, J. C. Liljegren, E. E. Clothiaux, K. E. Cady-Pereira, and K. L. Gaustad, 2007: Retrieving liquid water path and precipitable water vapor from the Atmospheric Radiation Measurement (ARM) microwave radiometers. *IEEE Trans. Geosci. Remote Sens.*, **45**, 3680–3690, https://doi.org/10.1109/TGRS.2007.903703.

Vial, J., J. L. Dufresne, and S. Bony, 2013: On the interpretation of inter-model spread in CMIP5 climate sensitivity estimates. *Climate Dyn.*, **41**, 3339–3362, https://doi.org/10.1007/s00382-013-1725-9.

Wallace, J. M., and P. V. Hobbs, 2006: *Atmospheric Science: An Introductory Survey*. 2nd ed. Elsevier, 488 pp.

Wang, M., H. Song, V. E. Larson, X. Dong, Z. Zhang, J. Wang, and P.-L. Ma, 2019: Subgrid variations of the cloud water and droplet number concentration over the tropical ocean: Satellite observations and implications for warm rain simulations in climate models. *Atmos. Chem. Phys.*, **19**, 1077–1096, https://doi.org/10.5194/acp-19-1077-2019.

Wood, R., 2005: Drizzle in stratiform boundary layer clouds. Part I: Vertical and horizontal structure. *J. Atmos. Sci.*, **62**, 3011–3033, https://doi.org/10.1175/JAS3529.1.

——, 2012: Stratocumulus clouds. *Mon. Wea. Rev.*, **140**, 2373–2423, https://doi.org/10.1175/MWR-D-11-00121.1.

——, T. L. Kubar, and D. L. Hartmann, 2009: Understanding the importance of microphysics and macrophysics for warm rain in marine low clouds. Part II: Heuristic models of rain formation. *J. Atmos. Sci.*, **66**, 2973–2990, https://doi.org/10.1175/2009JAS3072.1.

——, and Coauthors, 2015: Clouds, aerosols, and precipitation in the marine boundary layer: An ARM mobile facility deployment. *Bull. Amer. Meteor. Soc.*, **96**, 419–440, https://doi.org/10.1175/BAMS-D-13-00180.1.

Wu, P., X. Dong, and B. Xi, 2015: Marine boundary layer drizzle properties and their impact on cloud property retrieval. *Atmos. Meas. Tech.*, **8**, 3555–3562, https://doi.org/10.5194/amt-8-3555-2015.

——, ——, ——, Y. Liu, M. Thieman, and P. Minnis, 2017: Effects of environment forcing on marine boundary layer cloud-drizzle processes. *J. Geophys. Res. Atmos.*, **122**, 4463–4478, https://doi.org/10.1002/2016JD026326.

——, B. Xi, X. Dong, and Z. Zhang, 2018: Evaluation of autoconversion and accretion enhancement factors in general circulation model warm-rain parameterizations using ground-based measurements over the Azores. *Atmos. Chem. Phys.*, **18**, 17 405–17 420, https://doi.org/10.5194/acp-18-17405-2018.

——, X. Dong, B. Xi, J. Tian, and D. M. Ward, 2020: Profiles of MBL cloud and drizzle microphysical properties retrieved from ground-based observations and validated by aircraft in situ measurements over the Azores. *J. Geophys. Res. Atmos.*, **125**, e2019JD032205, https://doi.org/10.1029/2019JD032205.

Xie, X., and M. Zhang, 2015: Scale-aware parameterization of liquid cloud inhomogeneity and its impact on simulated climate in CESM. *J. Geophys. Res. Atmos.*, **120**, 8359–8371, https://doi.org/10.1002/2015JD023565.

Yamaguchi, T., G. Feingold, and J. Kazil, 2017: Stratocumulus to cumulus transition by drizzle. *J. Adv. Model. Earth Syst.*, **9**, 2333–2349, https://doi.org/10.1002/2017MS001104.

Yang, F., E. P. Luke, P. Kollias, A. B. Kostinski, and A. M. Vogelmann, 2018: Scaling of drizzle virga depth with cloud thickness for marine stratocumulus clouds. *Geophys. Res. Lett.*, **45**, 3746–3753, https://doi.org/10.1029/2018GL077145.

Yum, S. S., J. Wang, Y. Liu, G. Senum, S. Springston, R. McGraw, and J. M. Yeom, 2015: Cloud microphysical relationships and their implication on entrainment and mixing mechanism for the stratocumulus clouds measured during the VOCALS project. *J. Geophys. Res. Atmos.*, **120**, 5047–5069, https://doi.org/10.1002/2014JD022802.

Zelinka, M. D., T. A. Myers, D. T. McCoy, S. Po-Chedley, P. M. Caldwell, P. Ceppi, S. A. Klein, and K. E. Taylor, 2020: Causes of higher climate sensitivity in CMIP6 models. *Geophys. Res. Lett.*, **47**, e2019GL085782, https://doi.org/10.1029/2019GL085782.

Zhang, Z., H. Song, P. L. Ma, V. E. Larson, M. Wang, X. Dong, and J. Wang, 2019: Subgrid variations of the cloud water and droplet number concentration over the tropical ocean: Satellite observations and implications for warm rain simulations in climate models. *Atmos. Chem. Phys.*, **19**, 1077–1096, https://doi.org/10.5194/acp-19-1077-2019.